

## PDF hosted at the Radboud Repository of the Radboud University Nijmegen

The following full text is a preprint version which may differ from the publisher's version.

For additional information about this publication click this link.

<http://hdl.handle.net/2066/182907>

Please be advised that this information was generated on 2020-01-01 and may be subject to change.

# Finite Size Scaling in 2d Causal Set Quantum Gravity

Lisa Glaser<sup>a</sup>, Denjoe O’Connor<sup>b</sup> and Sumati Surya<sup>c</sup>

<sup>a</sup>Radboud University, Njimegen,

<sup>b</sup>DIAS, 10 Burlington Road Dublin 4 Ireland

<sup>c</sup> Raman Research Institute, CV Raman Ave, Bangalore, India,  
and Perimeter Institute, Waterloo, Canada

June 23, 2017

## Abstract

We study the  $N$ -dependent behaviour of 2d causal set quantum gravity. This theory is known to exhibit a phase transition as the analytic continuation parameter  $\beta$ , akin to an inverse temperature, is varied. Using a scaling analysis we find that the asymptotic regime is reached at relatively small values of  $N$ . Focussing on the 2d causal set action  $S$ , we find that  $\beta\langle S \rangle$  scales like  $N^\nu$  where the scaling exponent  $\nu$  takes different values on either side of the phase transition. For  $\beta > \beta_c$  we find that  $\nu = 2$  which is consistent with our analytic predictions for a non-continuum phase in the large  $\beta$  regime. For  $\beta < \beta_c$  we find that  $\nu = 0$ , consistent with a continuum phase of constant negative curvature thus suggesting a dynamically generated cosmological constant. Moreover, we find strong evidence that the phase transition is first order. Our results strongly suggest that the asymptotic regime is reached in 2d causal set quantum gravity for  $N \gtrsim 65$ .

## 1 Introduction

In causal set theory (CST) space-time is regarded as fundamentally discrete [1]. Approaching quantum gravity from this vantage point makes it possible to use computer simulations to explore non-perturbative features of the theory [2, 3, 4]. The system size that can be examined in computer simulations is always limited, and particularly so in CST, where non-locality leads to greater complexity. A finite size scaling analysis is therefore important in order to ensure that the results obtained for a given value of  $N$  can be generalized to larger

$N$ . Only if we find a convergence with  $N$  is it possible to generalize from finite values to the asymptotic regime.

Scaling with  $N$  is an important question for all lattice-type numerical simulations, whether in lattice gauge theory or quantum gravity, where large  $N$  convergence means that crossover transients due to finite size effects are suppressed. A standard way to assess this is to vary  $N$  and look for consistent scaling behaviour of relevant observables in order to extract scale invariant quantities. The physically reasonable assumption is that consistent scaling is evidence for asymptotic behaviour.

Such questions are of particular relevance to CST where numerical simulations of the dynamics are carried out for relatively small system size  $N$  [1, 2, 3, 4]. CST assumes a discrete or atomistic nature of spacetime as its fundamental kinematic hypothesis [1]. It is founded on the idea that discreteness and causality encode approximate Lorentzian geometry. Discreteness is implemented by replacing the spacetime continuum by locally finite partially ordered sets, or causal sets, with the order relation corresponding to the causal relation [1]. The condition of local finiteness captures the main hypothesis of the theory, namely that there is a *fundamental* spacetime discreteness or atomicity, so that every spacetime region of finite volume contains a finite number of causal set elements.

Causal sets that are approximated by the continuum are “random lattices” generated via a Poisson process. While this implies Lorentz invariance [5], it comes at the price of locality since the resulting graph is not of fixed or even finite valency. For example, a causal set that is approximated by Minkowski spacetime is not a finite valency graph; the combination of discreteness with Lorentz invariance ensures that every element in the causal set has infinite nearest neighbours. Non-locality is therefore a key feature of continuum-like causal sets and provides a promising avenue for phenomenological exploration [6, 7].

A major advance in the causal set program has been the development of a causal set version of the Einstein-Hilbert action — the Benincasa-Dowker (BD) action  $S$ , which incorporates this non-locality. The quantum partition function or sum-over-histories over the space of finite element causal sets can thus be constructed, with each causal set weighted by the quantum measure  $\exp(iS/\hbar)$ . This defines a theory of quantum gravity [2].

By introducing a parameter  $\beta$  akin to the inverse temperature this quantum partition function can be rendered into a Gibbs ensemble of finite element causal sets weighted by the BD action [8, 2]. This makes the theory amenable to numerical analysis and has yielded interesting results [2, 3, 4]. However, computational constraints arise when working with non-local graphs of large connectivity, and put practical limits on the size  $N$  of causal sets that can be used in numerical simulations. When simulating the quantum dynamics of causal sets using Markov Chain Monte Carlo (MCMC) algorithms, the non-locality increases the complexity drastically and slows down thermalisation times. The explorations of the parameter space to understand the asymptotic regime require a large number of independent simulations and are therefore resource demanding. While efforts are underway to improve algorithms, the fundamental limitation coming from the complexity of the graphs cannot be

easily overcome.

In light of this it becomes all the more important to understand the “finite size effects” in CST by examining the  $N$  dependence of various physically relevant quantities<sup>1</sup>. Extrapolating to large  $N$  helps in ascertaining macroscopic properties of the asymptotic regime, which can be relevant for the continuum approximation as well as for phenomenology.

Using MCMC methods it was shown in [2] that 2d CST exhibits two distinct phases as one varies over  $\beta \in \mathbb{R}^+$ . The high temperature phase is a continuum-like phase which we refer to as the  $\Pi_+$  phase and the other is a crystalline or non-continuum like phase, we label  $\Pi_-$  which occurs at low temperatures. The continuum like behaviour is consistent with the infinite temperature limit in which the system is known to be dominated by causal sets that are approximated by 2d Minkowski spacetime [9, 10]. The low temperature behaviour on the other hand is a new phase characterised by causal sets with very high graph connectivity, which has physically interesting consequences for the 2d Hartle-Hawking wave function, as shown in [3].

The results of [2] were obtained for causal sets with a few values of  $N$  and  $\epsilon$ , all of which showed the same qualitative features. However, no scaling analysis was done, and it was unclear if the phase transition would survive the large  $N$  limit. Indeed, it is the purpose of this paper to fill in this gap by doing a finite size scaling analysis and obtain convergence. In the process we are able to extract interesting physical information about the detailed nature of the phases and find strong evidence that the transition is first order.

Our principal results are

- For a fixed non-locality parameter  $\epsilon$ , the phase transition is shown to occur at a critical value  $\bar{\beta}_c$  of the rescaled inverse temperature  $\bar{\beta} = \beta N$ , where  $\bar{\beta}_c$  varies with  $\epsilon$  as  $\bar{\beta}_c \sim \frac{1}{\epsilon^2}$  in the large  $N$  limit.
- We find that for high, but finite, temperature the continuum phase is characterised by  $\langle S \rangle \propto N$  and corresponds to a constant negative curvature in the continuum approximation. We interpret this phase as an emergent anti-de Sitter space, which at infinite temperature becomes Minkowski space.
- In the small temperature phase we find that  $\langle S \rangle \propto N^2$ , which is consistent with our analysis that the zero temperature limit should be dominated by non-manifoldlike bilayered posets.
- We establish that the two phases are separated by a *first order* phase transition.
- The system enters the asymptotic regime for 2d CST for  $N \sim 65$ .

---

<sup>1</sup>Since discreteness is fundamental in CST, however, the attitude to finite size effects differs from theories in which discretisation is used as an ultraviolet regulator. Rather, the situation is similar to condensed matter physics where a finite value of  $N$ , however small, is *not* unphysical.

Our paper is organised as follows. In Section 2 we describe 2d CST in some detail and review the results of [2]. In Section 3 we define the large  $N$  asymptotic scaling exponents for  $\langle S \rangle$  on either side of the phase transition. We give analytic arguments for what the exponent should be in the limit of large  $\beta$ , based on the analysis of the action. In Section 4 we present the main results of this paper. We have generated an extensive data set using MCMC simulations for  $N$  ranging from 20 to 90 and for  $\epsilon$  ranging from 0.1 to 0.5, as shown in Table 1. This allows us to perform a detailed study and obtain not only the large  $N$  scaling of  $\langle S \rangle$  before and after the transition, but also an estimate for the function  $\langle S \rangle$  itself. We first show that the estimated critical inverse temperature  $\beta_c$  scales like  $N^{-1}$ . Using the rescaled inverse temperature  $\bar{\beta} = \beta N$ , we find that for the partition function  $Z$ ,  $\ln Z = -\beta F$  scales as  $-\bar{\beta} \bar{F} N^{\nu_{\pm}}$  (Eqn 10) with the scaling exponents  $\nu_+ = 1$ , and  $\nu_- = 0$  on either side of the phase transition. Hence we find that  $\ln Z$  is scale invariant before the phase transition and is extensive, i.e., scales with  $N$ , after the phase transition. Finally we demonstrate that the transition is of first order. In Section 5 we discuss some open questions.

## 2 A review of 2d causal set theory

### 2.1 Mathematical Preliminaries

We remind the reader of some key definitions in CST and refer them to the reviews [11, 12, 13] for more details. A *causal set*  $C$  is a locally finite partially ordered set. Thus  $C$  is a set with a relation  $\preceq$  which is (i) reflexive:  $x \preceq x$ , (ii) transitive:  $x \preceq y$  and  $y \preceq z$  implies  $x \preceq z$  (iii) acyclic:  $x, y \in C$  and  $x \preceq y \preceq x \Rightarrow x = y$  (iv) locally finite:  $|\text{Fut}(x) \cap \text{Past}(y)| < \infty$ , where  $\text{Fut}(x) \equiv \{z | x \prec z\}$  and  $\text{Past}(x) \equiv \{z | z \prec x\}$ .

The causal set hypothesis assumes that continuum spacetime is replaced by a discrete substratum, the causal set. A causal set  $C$  is said to have a *continuum approximation* to a spacetime  $(M, g)$  if  $C$  can be obtained from a Poisson sprinkling into  $(M, g)$  where  $P_v(n) = \frac{1}{n!}(\rho V)^n e^{-\rho V}$  is the probability of sprinkling  $n$  elements into a spacetime volume  $V$ .

Importantly, the assumption of a fundamental discreteness implies that the continuum limit itself is unphysical; it is only the continuum approximation that is physically relevant. Since discreteness is not used as a regulator for the continuum, finite size causal sets are not unphysical. The large  $N$  or asymptotic regime is phenomenologically interesting but not equivalent to the continuum regime.

We now write down some useful definitions.  $x, y \in C$  are said to be *linked* if  $x \prec y$  and  $\nexists z \in C$  such that  $x \prec z \prec y$ . A link is therefore an irreducible relation which cannot be obtained by transitive closure. A set  $A$  with no relations between the elements is called an *antichain* while a set  $B \equiv \{e_1, \dots, e_N\}$  which is totally ordered,  $e_1 \prec e_2 \prec \dots \prec e_N$  is called a *chain*.

An *interval*  $I(x, y) \equiv \{z | x \prec z \prec y\}$  is said to be an  *$n$ -element interval* if  $|I(x, y)| = n$ .

Thus if  $x \prec y$  is a link, then  $I(x, y)$  is a zero interval. The *abundance*  $N_n$  of  $n$ -element intervals in  $C$  is the number of such intervals in  $C$ .  $N_n$  is therefore an important covariant, or label independent, observable in  $C$ .

## 2.2 2d CST

The 2d BD action is

$$S(C, \epsilon) = 4\epsilon(N - 2\epsilon \sum_{n=0}^{N-2} N_n f(n, \epsilon)). \quad (1)$$

where  $N_n$  is the number of  $n$  element intervals and

$$f(n, \epsilon) = (1 - \epsilon)^n \left( 1 - \frac{2\epsilon n}{(1 - \epsilon)} + \frac{\epsilon^2 n(n - 1)}{2(1 - \epsilon)^2} \right). \quad (2)$$

This action depends on a non-locality scale  $l > l_p$ , the Planck scale, and where  $\epsilon = l_p^2/l^2 \in (0, 1]$ . This introduces  $\epsilon$  as a new free parameter or “coupling” that suppresses the fluctuations in the BD action in the continuum approximation.

In [14, 2] a two dimensional restriction of CST was defined by limiting the set of all causal sets to the set  $\Omega(N)$ , of  $N$  element “2d-orders”. These are causal sets that can be embedded into a causal diamond or Alexandrov interval in  $\mathbb{M}^2$ , via an order preserving map. Since the map need not be obtained from a Poisson sprinkling, not all causal sets in  $\Omega(N)$  have a continuum approximation.

Let us define our configurations more precisely. Beginning with a “base set”  $S = (1, \dots, N)$  let  $U = (u_1, u_2, \dots, u_N)$  and  $V = (v_1, v_2, \dots, v_N)$ , such that  $u_i, v_i \in S$ , with  $u_i = u_j \Rightarrow i = j$ , and  $v_i = v_j \Rightarrow i = j$ .  $U$  and  $V$  are therefore “totally ordered” by the integers, since every element is related to every other element. The 2d order  $C \equiv U \cap V$ , with  $e_i \equiv (u_i, v_i) \in C$  where  $e_i \prec e_j$  in  $C$  iff  $u_i < u_j$  and  $v_i < v_j$  [9, 10, 14].

Every 2d order embeds via an order preserving map into  $\mathbb{M}^2$  since the  $U, V$  orders provide a set of lightcone coordinates  $(u_i, v_i)$  for each element  $e_i$ . Conversely, every causal set obtained from a Poisson sprinkling into a topologically trivial interval in a 2d spacetime is a 2d order. Hence the sample space of 2d orders  $\Omega(N)$  includes all causal sets approximated by topologically trivial 2d spacetime regions as well as those that have no continuum approximation. While the unrestricted space of  $N$  element causal sets is known to be dominated by non-manifold like causal sets [15, 4] the restriction to 2d orders  $\Omega(N)$  was shown in [9, 10] to be dominated by the so-called “random” 2d orders, which are approximated by an interval in  $\mathbb{M}^2$  [14]. This makes the two dimensional restriction a good testing ground for non-perturbative causal set quantum gravity.

The quantum partition function is

$$Z(N) \equiv \sum_{C \in \Omega} e^{\frac{i}{\hbar} S(C, \epsilon)} \quad (3)$$

where  $S(C, \epsilon)$  is the 2d BD action (Eqn 1) with non-locality parameter  $\epsilon$ . Introducing an analytic continuation parameter  $\beta$  akin to the inverse temperature, we define a complex parameter family of partition functions

$$Z(\beta, N) \equiv \sum_{C \in \Omega} e^{-\frac{\beta}{\hbar} S(C, \epsilon)}. \quad (4)$$

Here  $\beta = -i$  is the quantum partition function while  $\beta \in \mathbb{R}^+$  is a statistical partition function (and a Gibbs ensemble of causal sets), which is amenable to numerical analysis. Note that the transition from the quantum to the statistical occurs without changing the sample space of causal sets, and hence the intrinsically Lorentzian character of configurations. This marks an important contrast with Euclidean methods and the usual Wick rotation procedure which renders the signature Euclidean, thus removing all trace of causality.

The equilibrium expectation value for any observable  $O$  in the Gibbs ensemble (Equation 3) is given by

$$\langle O \rangle_\beta = \frac{1}{Z} \sum_{C \in \Omega} O(C) e^{-\frac{\beta}{\hbar} S(C, \epsilon)} \quad (5)$$

and can be numerically obtained using Markov Chain Monte Carlo methods. In [2] the Markov Chain was generated via the following exchange move. Starting with any 2d order  $C = U \cap V$  with  $U = (u_1, u_2, \dots, u_N), V = (v_1, v_2, \dots, v_N)$ , a pair of distinct elements  $(i, j) \in S \times S, i \neq j$  are picked at random. Then picking  $U$  or  $V$  again at random, either  $u_i$  and  $u_j$  or  $v_i$  and  $v_j$  are exchanged (doing both will give back the original configuration). For example, starting with the 4-element chain  $U = (1, 2, 3, 4), V = (1, 2, 3, 4)$ , if  $i = 2, j = 3$  are picked in  $U$ , then the new 2d order is  $U = (1, 3, 2, 4), V = (1, 2, 3, 4)$ , for which the  $e_2, e_3$  elements are now spacelike, but to the past of  $e_4$  and the future of  $e_1$  forming a “diamond” causal set. This move satisfies detailed balance and is ergodic, as demonstrated explicitly in [2].

The expectation values of several covariant observables were calculated in [2], including the action, the abundance of intervals  $N_n$ , the number of maximal and minimal elements as well as the ordering fraction, whose inverse gives the Myrheim-Meyer estimate of the continuum spacetime dimension.  $\langle O \rangle_{\beta=0}$  for all these observables gave values consistent with the random 2d orders that dominate in the asymptotic limit [9, 10], which are approximated by 2d Minkowski spacetime. As  $\beta$  is increased, this continuum-like phase gives way, after a critical value  $\beta_c$ , to a non-manifold like phase characterised by “layered” causal sets shown in Figure 1. The phases are strikingly similar to what one might expect in an Ising model: at low temperatures ( $\beta > \beta_c$ ) the dominant phase is very regular, or crystalline, which resembles the ordered phase, while at high temperatures ( $\beta < \beta_c$ ) it is random, which resembles the disordered phase.

In Figure 2 we show results from new simulations, which plot  $\langle S \rangle$  as a function of  $\beta$  for various values of  $N$  and  $\epsilon$ . The phase transition is clearly visible even at  $N = 30$ . For a fixed  $\epsilon$ , as one varies over  $N$  the curves show a “sharpening” of the transition as  $N$  increases.

In [2] while several values of  $N$  and  $\epsilon$  were explored, the most extensive simulations were

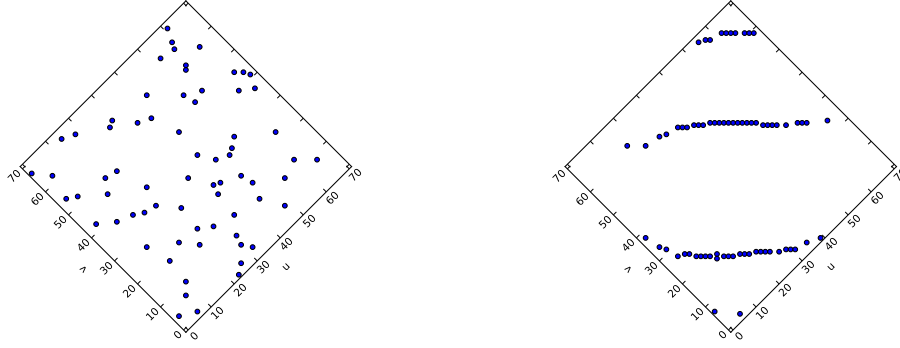


Figure 1: Examples of causal sets before ( $\beta = 0.008$ ) and after ( $\beta = 0.751$ ) the phase transition for  $N = 70$   $\epsilon = 0.2$ .

done only for a few values of  $N$  and  $\epsilon$ . The existing data was insufficient to deduce scaling behaviour with any confidence. In order to do so, we have for this work generated a far more extensive and comprehensive data set, which we have analysed along with the existing data. We find that plotting  $\langle S \rangle$  vs  $\beta N$  (see Figure 11) collapses the transition and the high temperature curve of  $\langle S \rangle$ , while plotting  $\langle S \rangle / N^2$  vs  $\beta N$  collapses the transition and the low temperature curve of  $\langle S \rangle$ . These prescriptions in general give excellent collapse on either side of the phase transition. Focusing on the high temperature continuum phase, we find that continuum phase does not correspond to flat spacetime, but instead has a non-zero, negative cosmological constant which decreases linearly with  $\beta$ , from the random 2d order at  $\beta = 0$ , up to the phase transition.

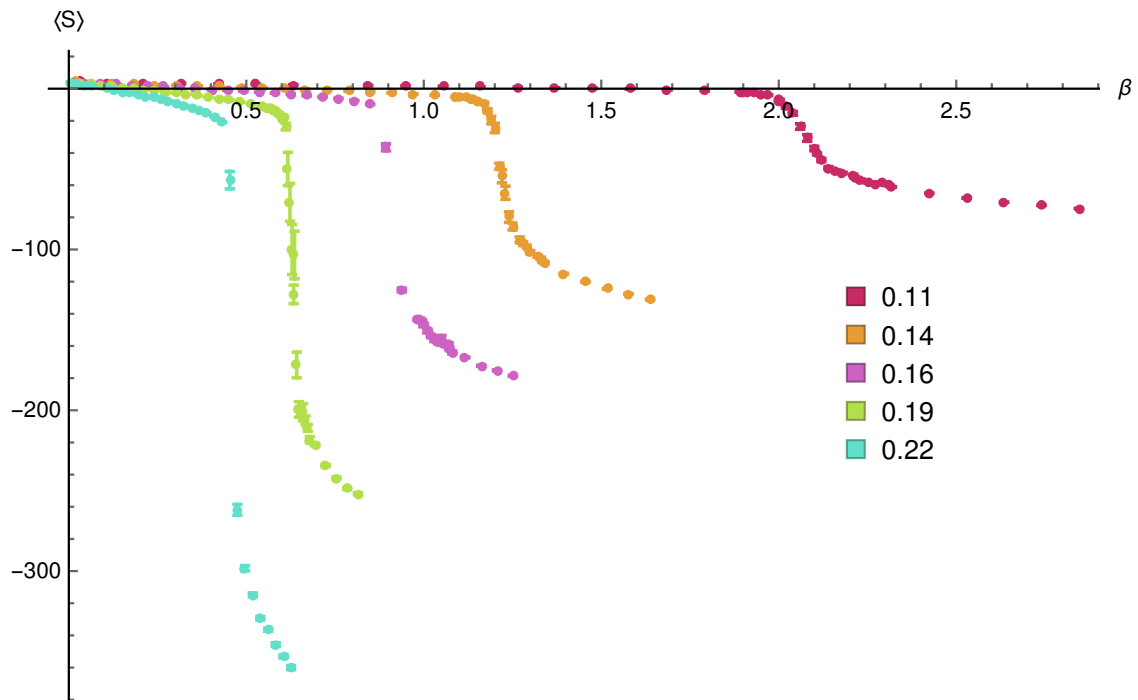
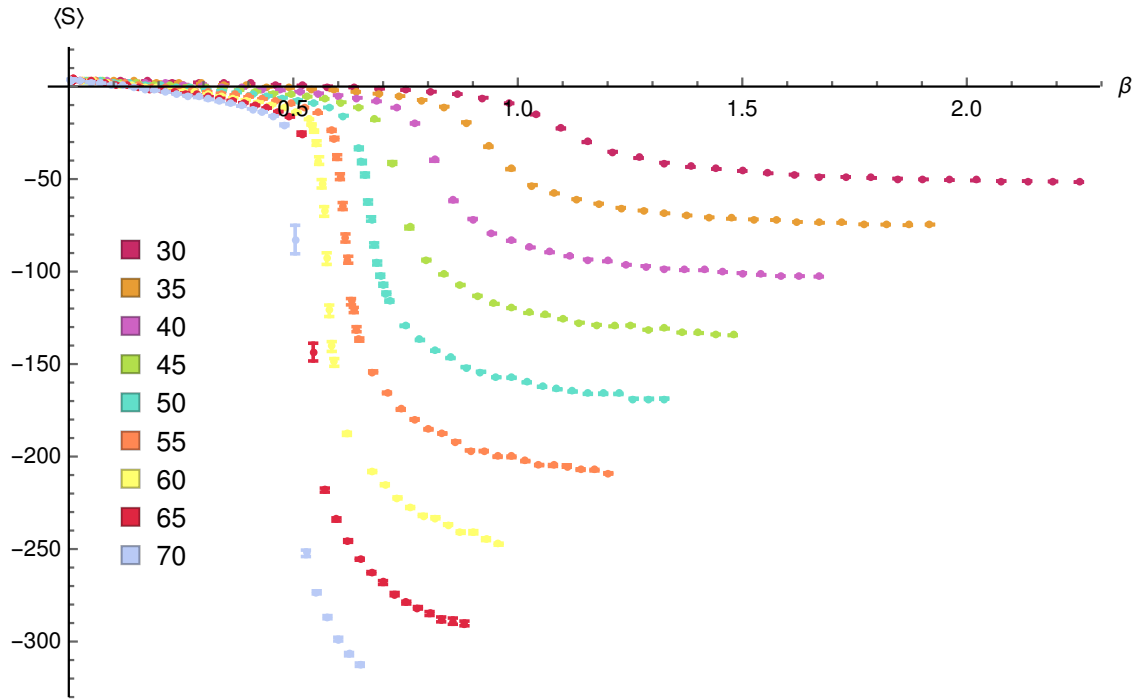


Figure 2: The first figure shows  $\langle S \rangle$  v/s  $\beta$  for various  $N$  values, for fixed  $\epsilon = 0.21$ . The second figure shows the same for various  $\epsilon$  values for fixed  $N = 70$ . The error bars on these graphs are very small, and hence appear as horizontal lines.

### 3 Scaling

Before embarking on analysing the data, we first lay the ground for our scaling analysis. We are interested in the scaling behaviour of the observable  $\langle S \rangle$  from which we can glean the scaling of the specific heat  $C$ . In terms of the free energy  $\beta F = -\ln Z$

$$\beta \langle S \rangle = \beta \frac{\partial(\beta F)}{\partial \beta}, \quad C = \beta^2 (\langle S - \langle S \rangle \rangle)^2 = -\beta^2 \frac{\partial^2(\beta F)}{\partial \beta^2}. \quad (6)$$

#### 3.1 Scaling in the small and large $\beta$ limit: an analytic argument

At  $\beta = 0$ ,  $\langle S \rangle$  is dominated by the ensemble of 2d random orders [9, 10] where  $\langle S \rangle \sim 4$  [16, 17]. Hence there is no scaling with  $N$  at  $\beta = 0$ . Assuming continuity of the partition function for small enough  $\beta$  the density of states will still dominate over the action. Indeed, Figure 2 indicates that  $\langle S \rangle$  is in fact a continuous function of  $\beta$ , suggesting that the deviation from flat spacetime and the continuum, if any, should occur continuously. If the deviation from flatness is approximately uniform for small enough  $\beta$ , with spatial variations in the curvature being picked up only at larger  $\beta$ , then one could expect  $S - 4 \propto N$ . This comes from a direct comparison with the continuum action for a constant curvature spacetime  $\frac{1}{16\pi G}RV$ , where  $R$  is the scalar curvature, and  $V$  the spacetime volume. In this case we would expect that for small enough  $\beta$  the scaling exponent is either 0 or 1. Indeed, no other scaling exponent has an obvious continuum or geometric interpretation.

In the opposite limit of large  $\beta$  on the other hand, the action dominates the density of states, and the dominant configuration is the one with the smallest energy. Now, the BD action (1) is not positive definite and its sign depends on the details of the causal set. The function  $f(n, \epsilon)$  (Eqn (2)) crosses over from being positive at small  $n$ , to negative for an intermediate range of values of  $n$  and then goes back to being positive. The precise location of the cross-over depends on  $\epsilon$  as shown in Figure 3. In particular,  $f(n, \epsilon)$  is positive and takes on its largest value when  $n = 0$ , i.e., for the links. This implies that the lowest energy causal sets have the the largest number of links. However, this energetic component has to compete with the density of states at finite  $\beta$ . At small  $\beta$ , the density of causal sets dominates the action. Indeed, the 2d random orders do not have the largest number of links  $N_0$  for a given  $N$ , and neither does the ensemble at small but non-zero  $\beta$  [2].

The class of 2d orders with the largest number of links for a given  $N$  are bilayer posets, i.e., those with  $\frac{N}{2}$  elements in each of the two layers, and such that every element in a layer is linked to all the elements in the other layer, as illustrated in Figure 4. For such posets,  $N_0 = \frac{N^2}{4}$ , with  $N_n = 0$  for all  $n > 0$ . The action has the simple form  $S = 4\epsilon N - 2\epsilon^2 N^2$  which scales like  $\sim N^2$  in the large  $N$  limit.

We can now compare the contribution to the partition function from the random orders  $Z_r(\beta, N, \epsilon)$  to that from these maximally connected bilayer posets  $Z_b(\beta, N, \epsilon)$ . If  $\rho_{r,b}(\beta, N, \epsilon)$

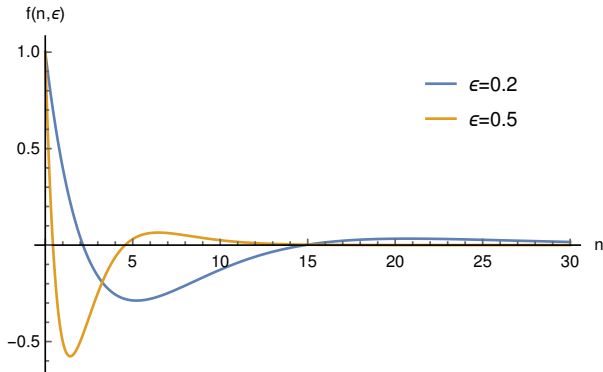


Figure 3: The function  $f(n, \epsilon)$  smears the contribution to the action from different  $n$ -element intervals. Larger  $\epsilon$  means less smearing.

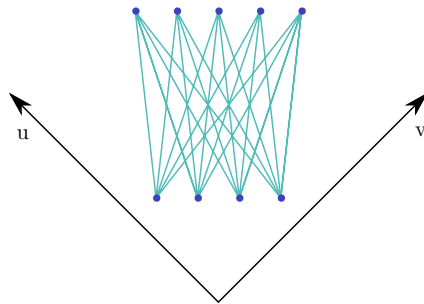


Figure 4: A bilayer causet with each element in the first layer linked to each elements in the second layer has the maximal possible number of links.

denote the respective density of states

$$Z_r(\beta, N, \epsilon) \equiv \rho_r(\beta, N, \epsilon) \sim N! \quad (7)$$

$$Z_b(\beta, N, \epsilon) \equiv \rho_b(\beta, N, \epsilon) e^{+2\beta\epsilon^2 N^2} \quad (8)$$

where we have used the results of [9, 10] for  $\rho_r(\beta = 0, N)$  and normalised by the common factor  $e^{-4\beta}$ . For  $\beta\epsilon^2$  large enough,  $Z_b$  will clearly dominate  $Z_r$  for large  $N$  irrespective of  $\rho_b$ .

This analysis suggests strongly that the dominant contribution to the partition function in the large  $\beta$  limit comes from bilayer posets and therefore that  $\langle S \rangle \sim N^2$  for large  $\beta$ .

### 3.2 Consistency

The scaling of  $\langle S \rangle$  and  $C$  must be consistent with the fact that they are both derived from the free energy  $F$  (Eqn (6)). In particular, away from the phase transition,  $\beta\langle S \rangle$  and  $C$  must have the same scaling exponents as  $\beta F$ .

To begin with, given that  $\beta_c$  seems to change with  $N$  in Figure 2, let us assume an  $N$ -dependence of  $\beta$  and define our first scaling exponent

$$\bar{\beta} = \beta N^\lambda, \quad (9)$$

where  $\bar{\beta}$  is scale independent to leading order in  $N$ . Then to leading order the scaling exponent for the free energy is given by

$$\beta F \sim \bar{\beta} \bar{F} N^\nu, \quad (10)$$

where  $\bar{F}$  is independent of  $N$ .  $\nu$  is therefore also the scaling exponent for  $\beta\langle S \rangle$  and  $C$ .

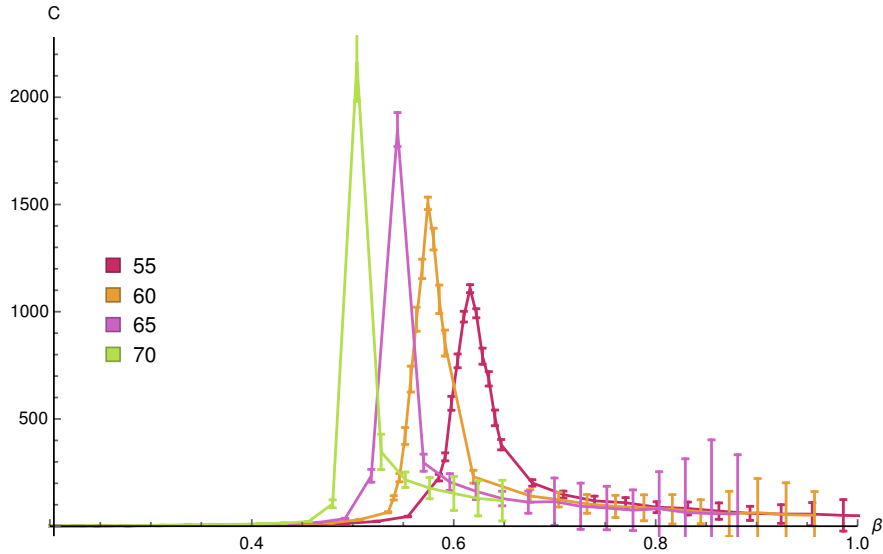


Figure 5: As  $N$  increases the peak in the specific heat  $C$  grows larger and sharper. The plot is for  $\epsilon = 0.21$ .

The scaling of the critical temperature  $\beta_c(N, \epsilon)$  with  $N$  should give  $\lambda$ , and the scaling of  $\beta\langle S \rangle$ ,  $\nu$ . In general, we should expect a different scaling for  $\beta\langle S \rangle$  (or  $\beta F$ ) on either side of the phase transition. Let  $\Pi_{\pm}$  refer to the phases  $\beta < (>)\beta_c$ , and  $\nu_{\pm}$  the respective critical exponents.

While the scaling exponents of  $C$  are also  $\nu_{\pm}$  away from the phase transition, *at* the phase transition the scaling depends on whether the transition is continuous or discontinuous. For a first order phase transition the first derivative of the free energy and hence  $\langle S \rangle$  is discontinuous. Figure 2 suggests this is a fair guess for our system since as  $N$  increases the transition becomes sharper, and  $C$  develops a singularity at the transition, which is consistent with Figure 5. Moreover we detect phase coexistence in a small region around the phase transition, Figure 6.

However, *establishing* a discontinuity or a singularity in a finite system requires more than such indications. Indeed, as pointed out in [18], a finite peak is seen for both first and second order transitions in finite systems. Additionally, phase coexistence occurs in finite systems for both types of transitions, and result in double Gaussians in the frequency histograms of the order parameters. The distinguishing feature is that the double Gaussians persist and become more pronounced in a first order phase transition as  $N$  is increased, while for a second order phase transition the two begin to merge. Indeed, this is what our data shows as we will demonstrate in Section 4.

The nature of the phase transition affects the scaling of  $C$  with  $N$  at the phase transition. For a second order phase transition, since the distribution goes over to a single Gaussian, the scaling of  $C$  is the same as that of  $\beta\langle S \rangle$  in this regime. This also means that the scaling of  $\beta\langle S \rangle$  must be the same across the transition. However, this is not true for a first order phase

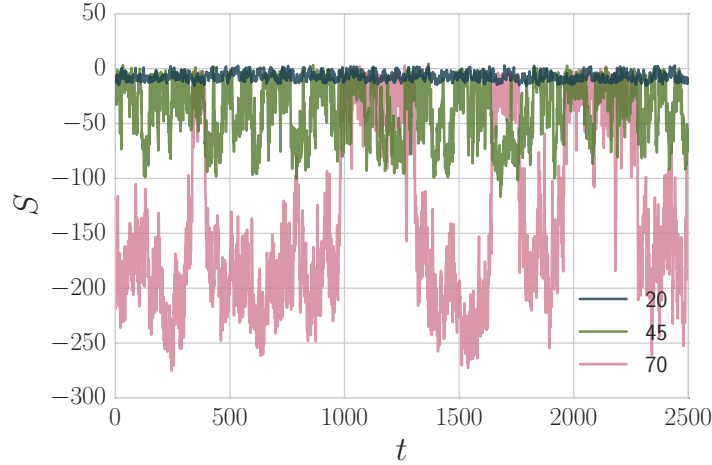


Figure 6: The coexistence of different phases at the phase transition for fixed  $\epsilon = 0.2$ ,  $N = 20, 45, 70$  with the Markov chain jumping between the two phases. With larger  $N$  the difference in action of the regions becomes larger and jumps become less frequent, but more pronounced.

transition, where the coexistence of phases is characterised by two well separated Gaussians, each with a given mean and variance. The probability distribution for any observable  $x$  at a given  $\beta$  is therefore

$$P(x) = p_+(\beta)P_G(x, \mu_+, \sigma_+, \beta) + p_-(\beta)P_G(x, \mu_-, \sigma_-, \beta), \quad (11)$$

where  $P_G(x, \mu_{\pm}, \sigma_{\pm}, \beta)$  are themselves Gaussians with mean  $\mu_{\pm}$  and standard deviation  $\sigma_{\pm}$ .  $p_{\pm}(\beta)$  are the relative frequency configurations in  $\pi_{\pm}$  in the ensemble, at a given  $\beta$ . For  $\beta < \beta_c$  away from the transition,  $p_-(\beta)$  goes to zero, and similarly for  $\beta > \beta_c$ , again away from the transition,  $p_+(\beta)$  goes to zero so that away from the phase transition, Gaussianity is restored.

At (and near) a first order phase transition the deviation from Gaussianity, Eqn (11) affects the scaling behaviour. For the action  $S$ ,

$$\langle S \rangle = p_+ \langle S_+ \rangle + p_- \langle S_- \rangle, \quad (12)$$

while the specific heat

$$C = p_+ p_- (\beta \langle S_+ \rangle - \beta \langle S_- \rangle)^2 + p_+ \beta C_+ + p_- \beta C_-. \quad (13)$$

where  $\langle S_{\pm} \rangle$  and  $C_{\pm}$  are the average  $S$  and  $C$  in  $\Pi_{\pm}$ , respectively. Given the scaling on either side of the phase transition

$$\beta \langle S_{\pm} \rangle \sim \beta \langle \bar{S}_{\pm} \rangle N^{\nu_{\pm}} \quad (14)$$

we expect

$$C_{\pm}(\beta, N, \epsilon) \sim \bar{C}_{\pm}(\bar{\beta}, \epsilon) N^{\nu_{\pm}}. \quad (15)$$

On the other hand, Eqn (13) implies that

$$C(\beta, N, \epsilon) \sim \bar{C}(\bar{\beta}, \epsilon) N^{2\nu}. \quad (16)$$

where  $\nu$  denotes the larger of  $\nu_{\pm}$ .

## 4 Results

Our MCMC code was used to generate  $\langle S \rangle$  for the values of  $N$  and  $\epsilon$  given in Table 1. For each  $N, \epsilon$  there were at a minimum, 35 values of  $\beta$  that were explored, so that the total number of data points generated was over 6000. Moreover, for each data point there were 20,000 sweeps, each sweep having  $N(N-1)/2$  attempted MCMC moves. These simulations were done on the HPC at the Raman Research Institute.

The first set of simulations were done over  $\beta$  values evenly spread out from  $\beta = 0$  to the maximum possible  $\beta > \beta_c$ , this being determined by thermalisation times. The next set of simulations was focused on the critical region. For some  $N, \epsilon$  values we even did a third refinement. Each set of simulations took several weeks on the RRI HPC cluster. The aim was to span the parameter space rather than focus on fixed  $N$  and  $\epsilon$ .

Importantly, our data shows that the *qualitative* behaviour is unchanged as  $N$  and  $\epsilon$  are varied with the appearance of a phase transition from one distinct phase into another as  $\beta$  is varied. Figure 2 uses this new data giving  $\langle S \rangle$  as a function of  $\beta$  for both a fixed  $\epsilon (= 0.21)$  and varying  $N$ , and also for fixed  $N (= 70)$  and varying  $\epsilon$ . From these it is apparent that for fixed  $\epsilon$  the critical inverse temperature  $\beta_c$  decreases with  $N$ , and similarly for fixed  $N$ , it decreases with  $\epsilon$ . These graphs show a strong hint of scaling, but it is clear that this is non-trivial. A seeming worry is that as  $N$  increases,  $\beta_c$  goes to 0, so that the phase transition appears to vanish in the asymptotic regime. However, we now show that when rescaled as  $\bar{\beta} = \beta N$ , the rescaled  $\bar{\beta}_c$  rapidly converges to a fixed value with  $N$ .

We note that in order for the BD action to yield the right continuum approximation,  $\epsilon$  must be large enough for a given  $N$ , otherwise the non-locality scale  $l_p/\sqrt{\epsilon}$  will exceed the IR cut off. In this case, the BD action will not yield the Einstein Hilbert action in the continuum approximation and hence is not quantum gravity as we have defined it. Thus there exists a smallest  $\epsilon_0$  for every  $N$ . The expectation is that  $\epsilon_0(N) \sim N^{-c}$  for  $c > 0$ , so that  $\epsilon_0(N) \rightarrow 0$  as  $N \rightarrow \infty$ . In analysing our data this cut-off was taken into account.

Table 1: Values of  $N$  and  $\epsilon$  used in our analysis

$N$	$\epsilon$									
30	0.1	0.11	0.12	0.13	0.14	0.15	0.16	0.17	0.18	0.19
	0.2	0.21	0.22	0.23	0.24	0.25	0.3	0.35	0.4	0.5
35	0.1	0.11	0.12	0.13	0.14	0.15	0.16	0.17	0.18	0.19
	0.2	0.21	0.22	0.23	0.24	0.25	0.3	0.35	0.4	0.5
40	0.1	0.11	0.12	0.13	0.14	0.15	0.16	0.17	0.18	0.19
	0.2	0.21	0.22	0.23	0.24	0.25	0.3	0.35	0.4	0.5
45	0.1	0.11	0.12	0.13	0.14	0.15	0.16	0.17	0.18	0.19
	0.2	0.21	0.22	0.23	0.24	0.25	0.3	0.35	0.4	0.5
50	0.1	0.11	0.12	0.13	0.14	0.15	0.16	0.17	0.18	0.19
	0.2	0.21	0.22	0.23	0.24	0.25	0.3	0.35	0.4	0.5
55	0.1	0.11	0.12	0.13	0.14	0.15	0.16	0.17	0.18	0.19
	0.2	0.21	0.22	0.23	0.24	0.25	0.3	0.35	0.4	0.5
60	0.1	0.11	0.12	0.13	0.14	0.15	0.16	0.17	0.18	0.19
	0.2	0.21	0.22	0.23	0.24	0.25	0.3	0.35	0.4	0.5
65	0.1	0.11	0.12	0.13	0.14	0.15	0.16	0.17	0.18	0.19
	0.2	0.21	0.22	0.23	0.24	0.25	0.3	0.35	0.4	0.5
70	0.1	0.11	0.12	0.13	0.14	0.15	0.16	0.17	0.18	0.19
	0.2	0.21	0.22	0.23	0.24	0.25	0.3	0.35	0.4	0.5
75	0.11									
80	0.11	0.12	0.13	0.14	0.15	0.16	0.17	0.18	0.19	
90	0.11	0.13	0.14	0.15						

## 4.1 Scaling of $\beta$

We estimate  $\beta_c$  as the location of the maxima of the (simulated) value of the specific heat  $C$ . Clearly, the real maximum could lie at a value of  $\beta$  which we did not simulate and hence it is important to assess the error  $\Delta\beta_c$ . We take this to be the largest interval on the  $\beta$  axis which contains  $\beta_c$ , such that the errors in  $C$  of the end point values of the interval overlap with the errors in  $C$  at  $\beta_c$ . We illustrate this in 7.

Our data suggests a scaling  $\beta_c \sim \frac{1}{N\epsilon^2}$  as shown in Figure 8. Assuming

$$\beta_c = \frac{b(\epsilon)}{N} + \frac{c(\epsilon)}{N^2} + O\left(\frac{1}{N^3}\right), \quad (17)$$

we find fits for  $b(\epsilon)$  and  $c(\epsilon)$  as shown in Figs 9,

$$b(\epsilon) = \frac{1.66(\pm 0.03)}{\epsilon^2}, \quad c(\epsilon) = \frac{4.09(\pm 0.50)}{\epsilon^3} - \frac{27.77(\pm 2.45)}{\epsilon^2} \quad (18)$$

Using these estimates for  $b(\epsilon)$  and  $c(\epsilon)$ , we find very good fit with the data as shown in Figure 10. Thus, to leading order, we can define the scale invariant temperature  $\bar{\beta} \sim \beta N$ . Replotting  $\langle S \rangle$  v/s  $\bar{\beta}$  we find a strong convergence to  $\bar{\beta}_c$  as  $N$  increases as shown in Figure 11.

This yields the first exponent  $\lambda = -1$ .

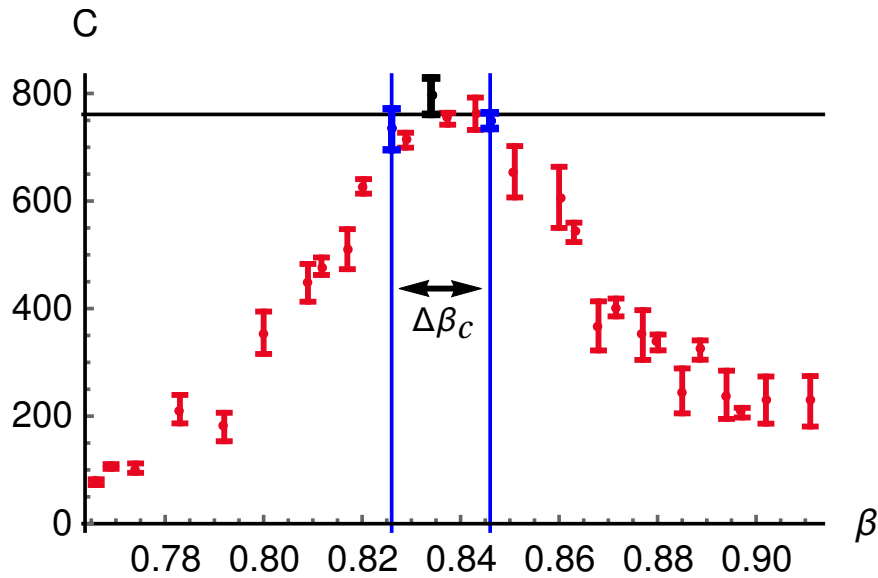


Figure 7: We take the pseudocritical point  $\beta_c$  to be the location of the maxima of  $C$ . To estimate the error  $\Delta\beta_c$  we compare the error in  $C_{\max}$  at  $\beta_c$  with that of neighbouring points. The two  $\beta$  values on either side of  $\beta_c$  which are furthest away from it and such that their errors in  $C$  overlap with that at  $C_{\max}$  then determine  $\Delta\beta_c$ .

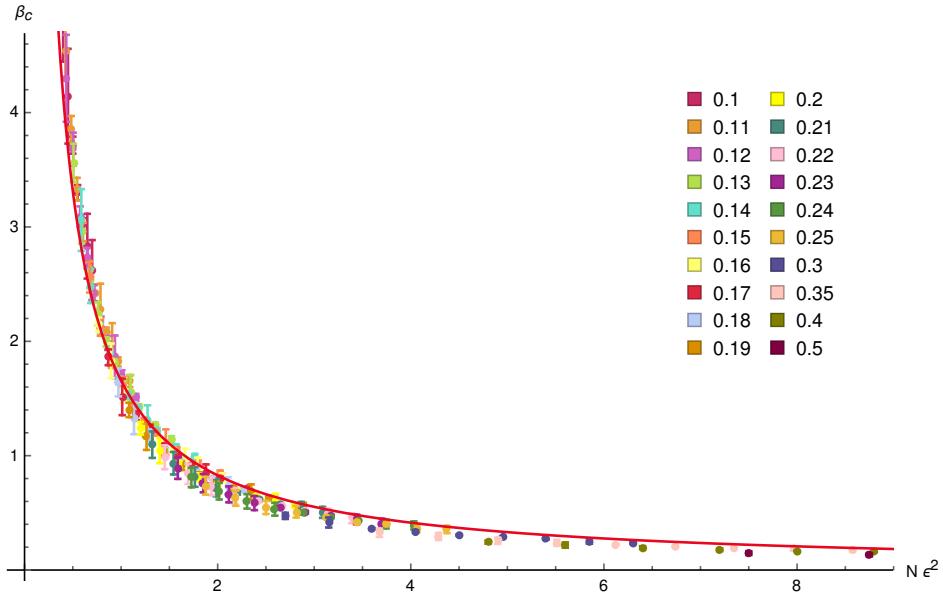


Figure 8: We show  $\beta_c$  against  $N\epsilon^2$ , and see that the data collapses very well for all values of  $N, \epsilon$ .

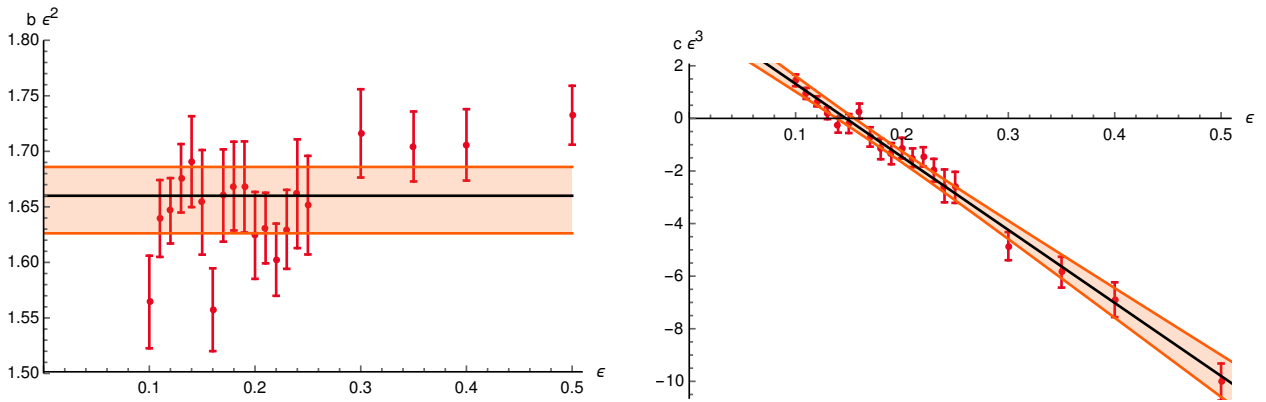


Figure 9: Best fits for  $b, c$  as functions of  $\epsilon$ .

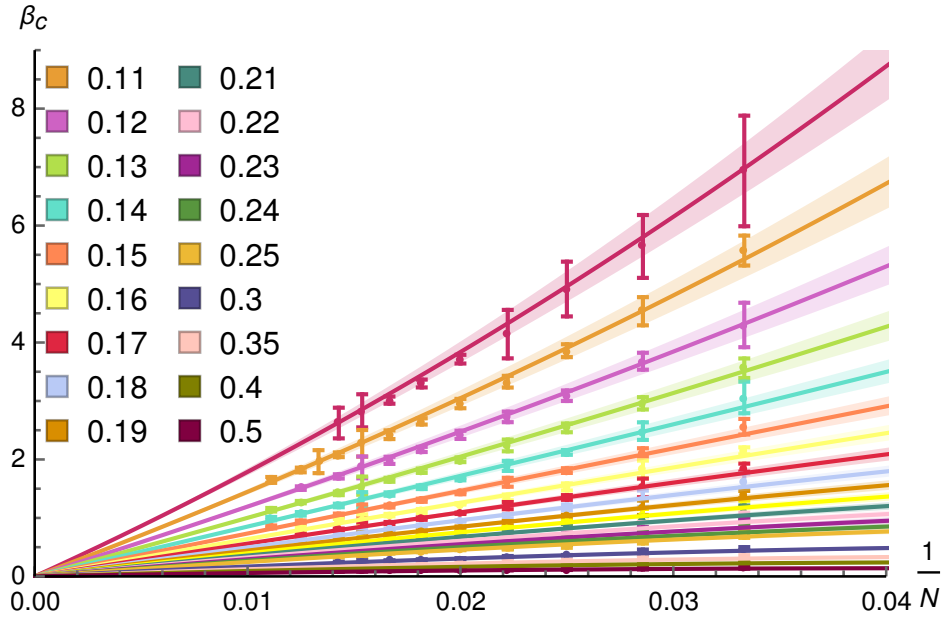


Figure 10: Plotting  $\beta_c$  vs  $\frac{1}{N}$  shows a clear linear dependence. The lines are plotted using equation (17), and the shaded region shows the 99% confidence interval.

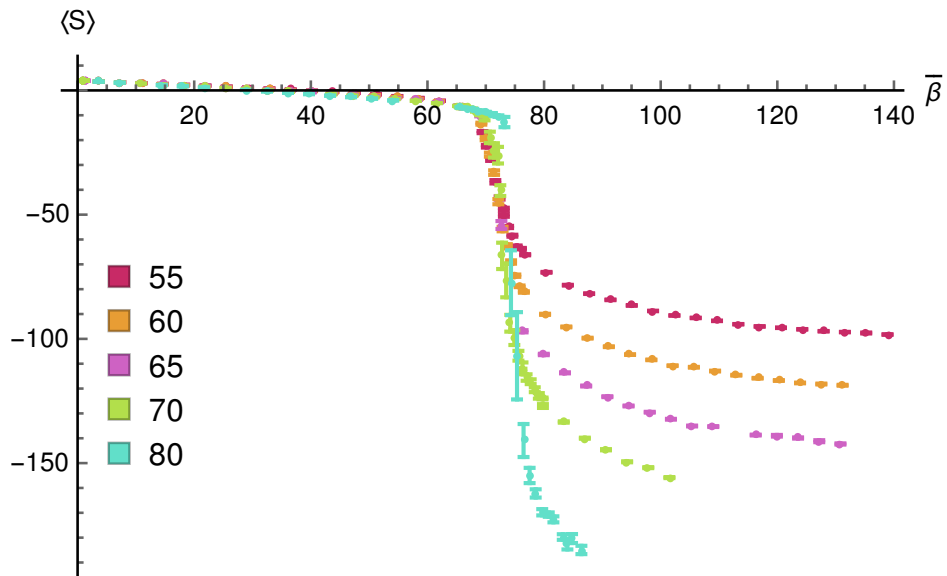


Figure 11: This figure shows how for  $\epsilon = 0.15$  the rescaled critical temperature  $\bar{\beta} = \beta N$  converges for larger  $N$ . Again, the error bars are very small, and show up as lines in the graph.

## 4.2 Scaling of $\langle S \rangle$

We now examine the scaling of  $\langle S \rangle$  in the phases  $\Pi_{\pm}$  to estimate the scaling exponents  $\nu_{\pm}$ .

In the continuum phase  $\Pi_{-}$  region we see that rather than staying constant as one might expect for the 2d random order,  $\langle S \rangle$ , drops away from 0 with a linear dependence on  $\bar{\beta}$ , as shown in Figure 12. To leading order we guess that

$$\langle S \rangle - 4 = b^{-}(N, \epsilon)\bar{\beta}, \quad (19)$$

with

$$b^{-}(N, \epsilon) = b_1^{-}(\epsilon)N + b_0^{-}(\epsilon) \quad (20)$$

In Figures 13 we find fits for  $b_0^{-}(\epsilon)$  and  $b_1^{-}(\epsilon)$  and find that

$$\begin{aligned} b_1(\epsilon) &= -0.20(\pm 0.06)\epsilon^3 - 2.04(\pm 0.18)\epsilon^4 \\ b_0(\epsilon) &= 2.09(\pm 0.55)(\epsilon - 0.07(\pm 0.01))^2 - 190.50(\pm 15.46)(\epsilon - 0.07(\pm 0.01))^4. \end{aligned} \quad (21)$$

The plots also show the 99% confidence interval for the fits. In Fig 20 we divide the average action by the best fit function to show the goodness of the fit.

To leading order, then,  $\langle S \rangle \sim N$ . This is interesting since for the 2d random orders, the action does not scale with  $N$ , i.e.,  $\langle S \rangle \sim 4$  for all  $N$ . Therefore, it is evident that the ‘‘continuum’’ phase is *not* dominated by flat spacetime for  $\bar{\beta} > 0$ . As we will discuss in Section 5 this scaling is consistent with a constant curvature spacetime of negative curvature, i.e.,  $\text{adS}_2$ . We show further support for this, which suggests that 2d CST has a dynamical mechanism for generating a cosmological constant.

Since  $\beta$  itself scales as  $N^{-1}$ , this means that  $\beta\langle S \rangle \sim N^0$ , or that  $\nu_{-} = 0$  as is clear from the convergence of the larger values of  $N$  shown in Figure 15. We can do more in this case. To leading order since

$$-\bar{\beta} \frac{\partial}{\partial \bar{\beta}} \ln Z \sim b_1^{-}(\epsilon)\bar{\beta}^2 \quad (22)$$

we see that the free energy  $\beta F$  is scale invariant and hence non-extensive. This expression is in fact so simple, we can integrate it to find the partition function

$$\ln \frac{Z}{Z_0} \sim - \int_0^{\bar{\beta}} b_1^{-}(\epsilon)\bar{\beta}' d\bar{\beta}' = -\frac{1}{2}b_1^{-}(\epsilon)\bar{\beta}^2. \quad (23)$$

Here,  $Z_0$  is the partition function at  $\beta = 0$  which to leading order in  $N$ , is given by the density of states  $N!$  for the 2d random orders (Eqn 7).

At the other end, for  $\beta > \beta_c$ ,  $\langle S \rangle$  changes with  $N$ , becoming more and more negative as  $N$  increases as shown in Figure 16(a). In Figure 16(b) we plot  $\beta\langle S \rangle/N$  with  $\bar{\beta}$  and find a linear behaviour with  $\bar{\beta}$  which converges with increasing  $N$ . Modelling the linear behaviour as

$$\beta\langle S \rangle = a^{+}(N, \epsilon) + b^{+}(N, \epsilon)\bar{\beta}, \quad (24)$$

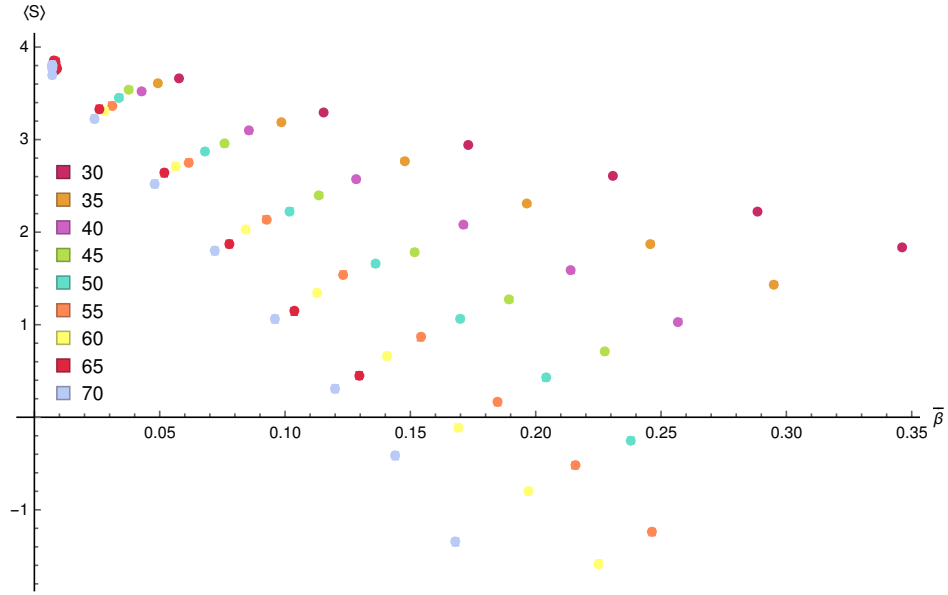


Figure 12:  $\langle S \rangle$  as a function of  $\bar{\beta}$  before the phase transition and the linear best fits for  $\epsilon = 0.21$ .

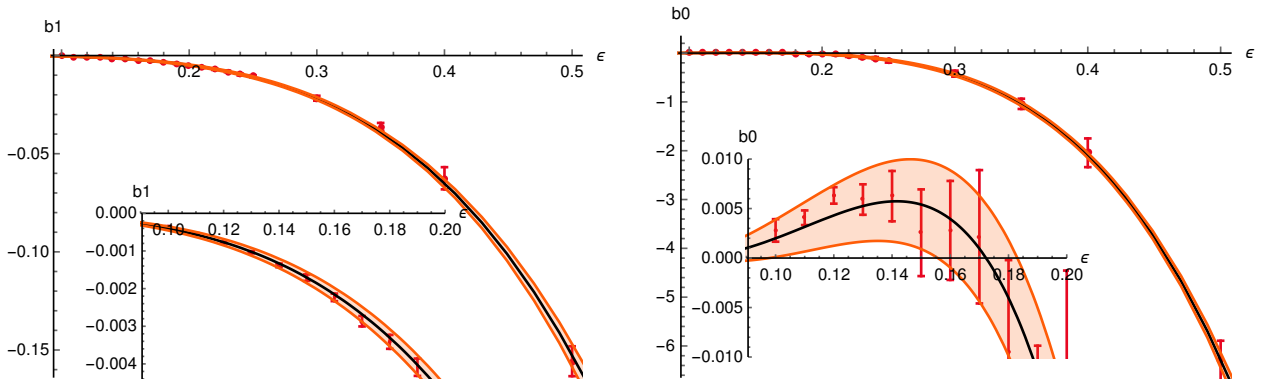


Figure 13: Best fits and confidence regions for  $b_1(\epsilon), b_0(\epsilon)$ . The inlays show a zoom for the small  $\epsilon$  region.

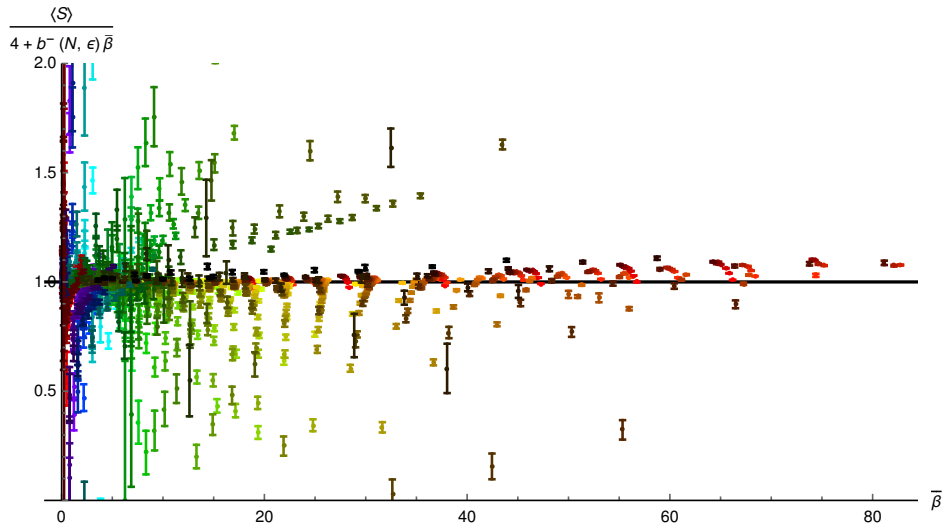


Figure 14: Dividing the average action by the best fit function for the region before the phase transition (19) shows a very good fit for all ranges of  $N, \epsilon$ . The color shows the value of  $\epsilon$  (with  $\epsilon$  decreasing from left to right), while the brightness indicates  $N$ , with darker dots indicating larger  $N$  values.

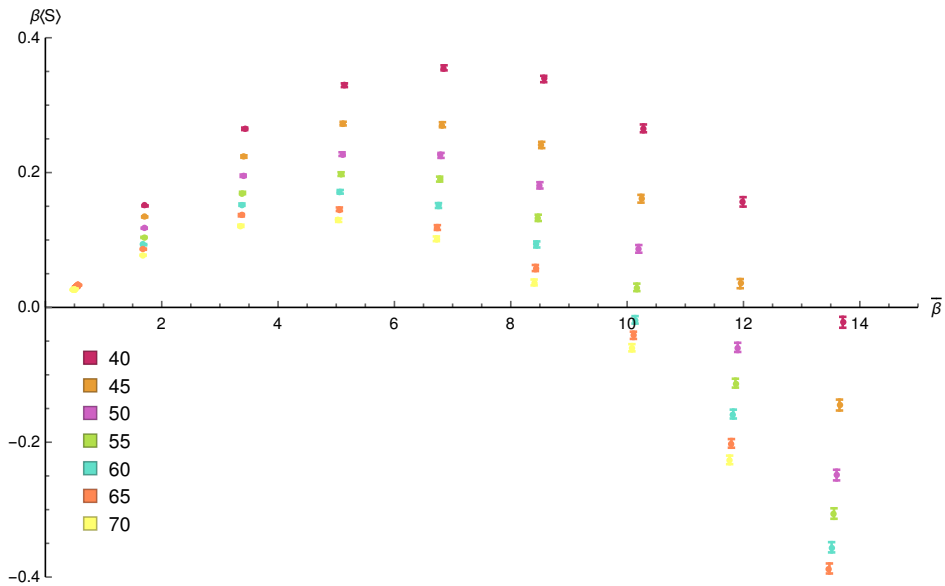


Figure 15: In the phase  $\Pi_-$ ,  $\beta\langle S \rangle$  shows a convergence for large  $N$ .

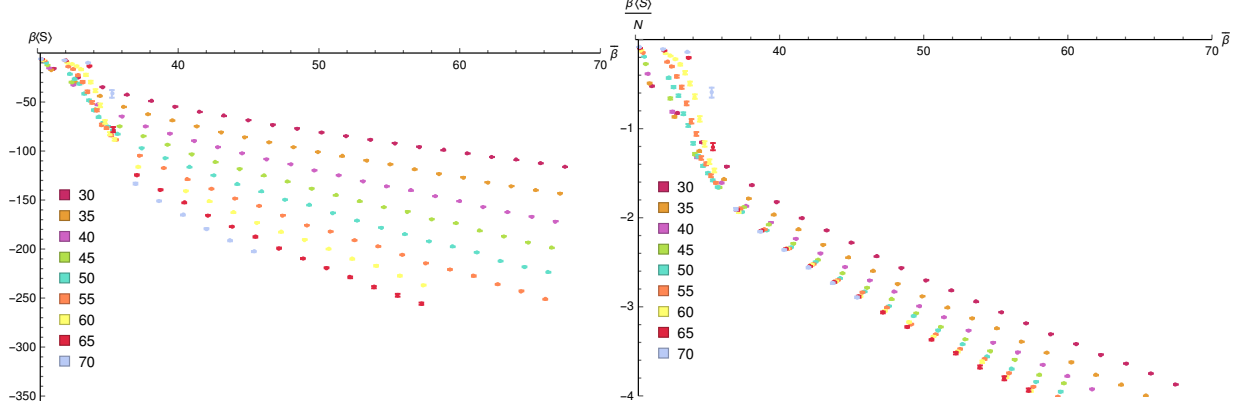


Figure 16: In the phase  $\Pi_+$ , we see  $\beta\langle S \rangle$  behaves linearly with  $\bar{\beta}$  in the figure on the left. On the right we show it rescaled as  $\beta\langle S \rangle/N$  which shows convergence for large  $N$ .

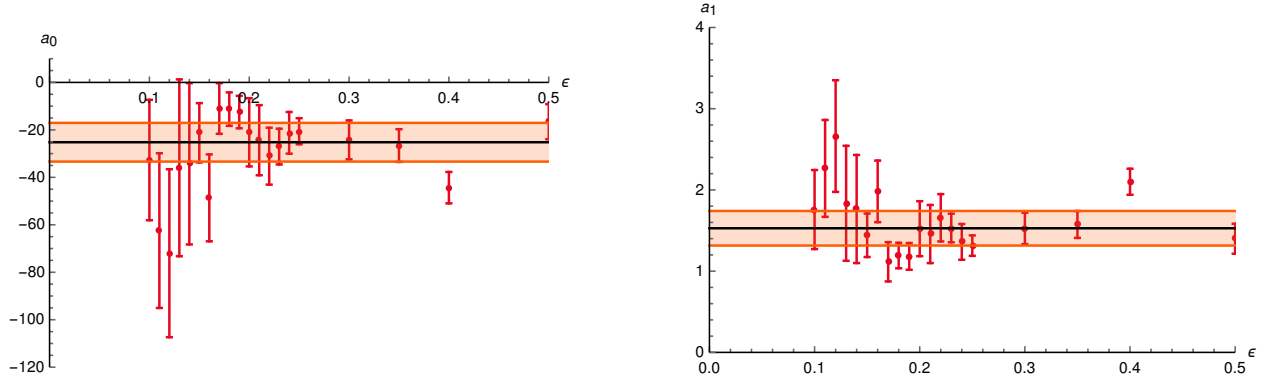


Figure 17: Best fits for  $a_0$  and  $a_1$  as functions of  $\epsilon$  and 99 % confidence intervals.

we let

$$a^+(N, \epsilon) = a_0^+(\epsilon) + a_1^+(\epsilon)N, \quad b^+(N, \epsilon) = b_0^+(\epsilon) + b_1^+(\epsilon)N. \quad (25)$$

In Figures 17,18 we show the best fits for these functions and find that

$$a^+(N, \epsilon) = -25.21(\pm 8.16) + 1.53(\pm 0.21)N, \quad (26)$$

$$b^+(N, \epsilon) = 0.4(\pm 0.24) + 17.63(\pm 4.76)\epsilon^2 - 2.48(\pm 0.09)\epsilon^2 N. \quad (27)$$

We plot Equation (24) with these fits in Fig 19 and find them to be in good agreement with the data.

We conclude that  $\nu_+ = 1$ , which implies that the free energy  $\beta F$  scales as  $N$  in this phase and is hence extensive. Notice that this is consistent with our expectations in the large  $\beta$  limit, where  $S$  for the bilayer poset scales as  $N^2$ .

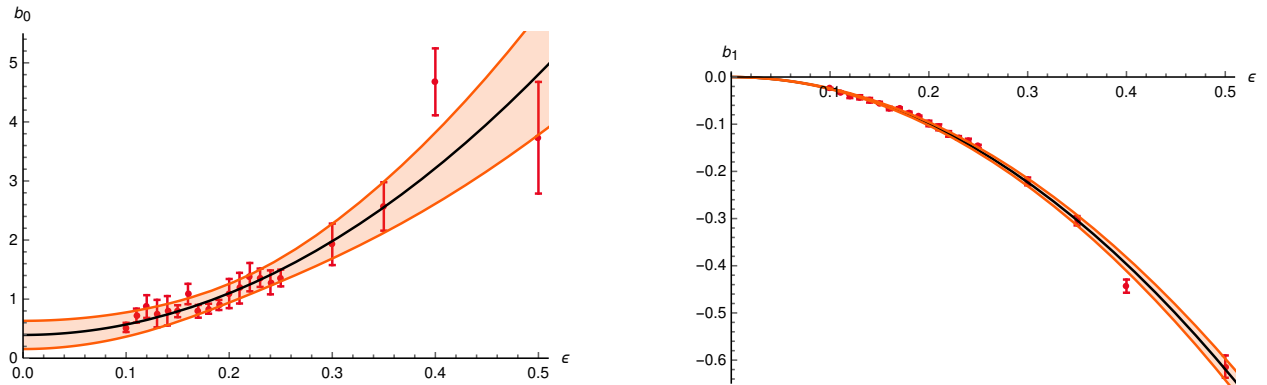


Figure 18: Best fits for  $b_0$  and  $b_1$  as functions of  $\epsilon$ .

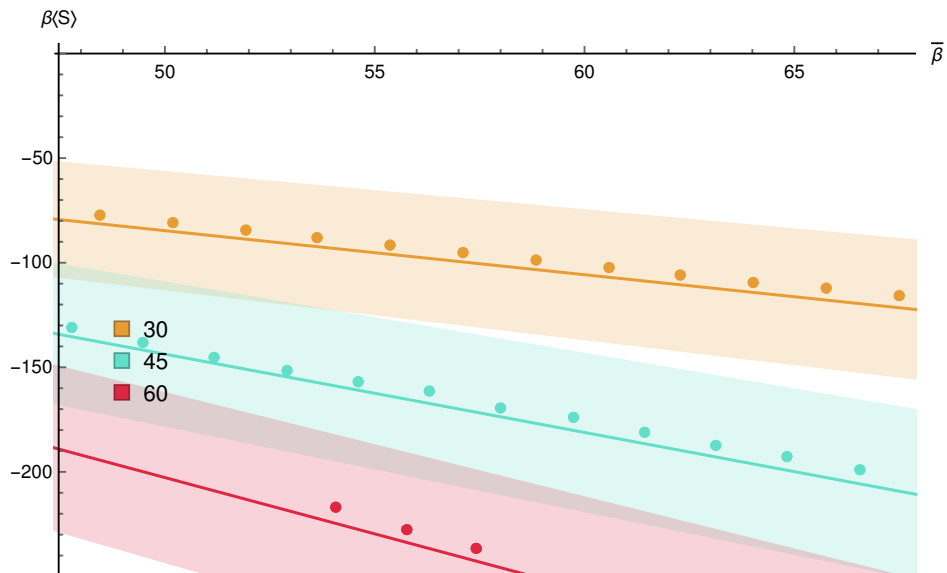


Figure 19: Plotting the fit using equation (26) against the data we see good agreement with the data, shown here for  $\epsilon = 0.21$ . We plot a few values of  $N$  to avoid too much overlap in the 99% uncertainty region.

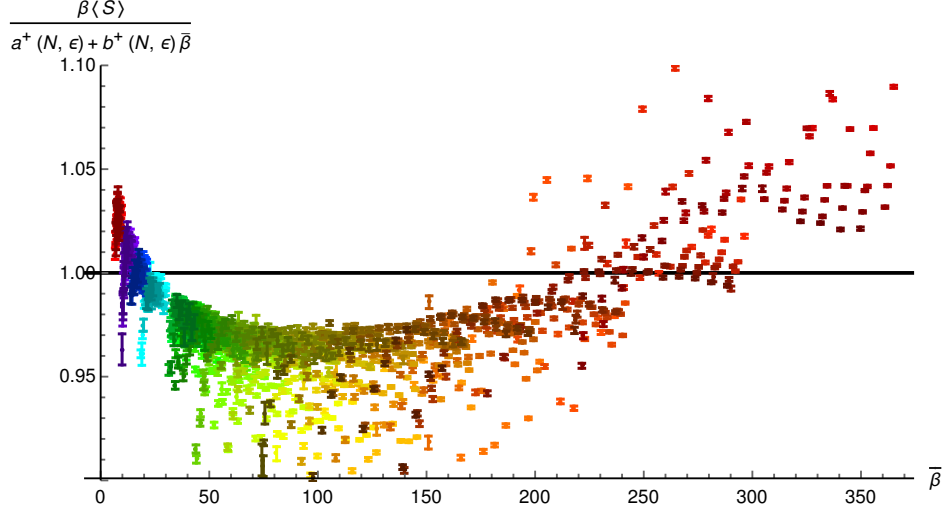


Figure 20: Dividing the average action times  $\beta$  by the best fit function for the phase  $\Pi_+$  (24) shows a very good fit for all ranges of  $N, \epsilon$ . The color shows the value of  $\epsilon$  (with  $\epsilon$  decreasing from left to right), while the brightness indicates  $N$ , with darker dots corresponding to larger  $N$ .

We note that this behaviour is reminiscent of the two phases in the dimer model of [19] where again  $\beta F$  is scale invariant in one phase and extensive in the other phase.

We now look at the specific heat plots to check the consistency of our analysis. Given that

$$C = -\beta^2 \frac{\partial \langle S \rangle}{\partial \beta} = -\frac{\bar{\beta}^2}{N} \frac{\partial \langle S \rangle}{\partial \bar{\beta}} \quad (28)$$

we see that to leading order in  $N$

$$C_- = -b_1^-(\epsilon) \bar{\beta}^2, \quad C_+ = a_1^+(\epsilon) N \quad (29)$$

The unscaled plots in the two regions are given in Figure 21. In the  $\Pi_-$  region a collapse is fairly clear, without the need for scaling. On the other hand, the  $\Pi_+$  region collapses when one scales by  $N$  as shown in Figure 22. The largest values of  $N$  show the convergence for the respective scalings in the two regions.

Plotting the fit lines from eqn (29) doesn't lead to convincing plots. This is presumably because next to leading order corrections become important further from the phase transition for  $C$  than for  $\langle S \rangle$ .

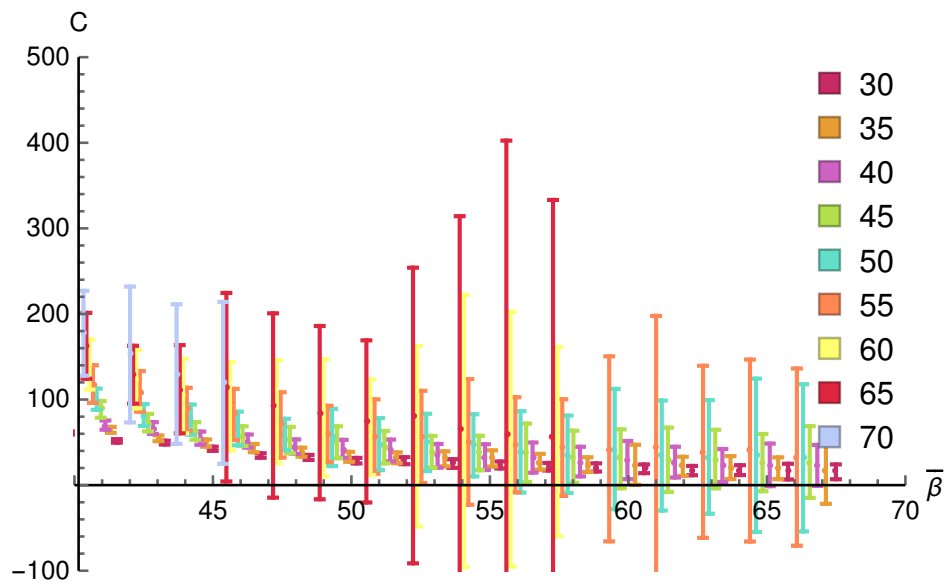
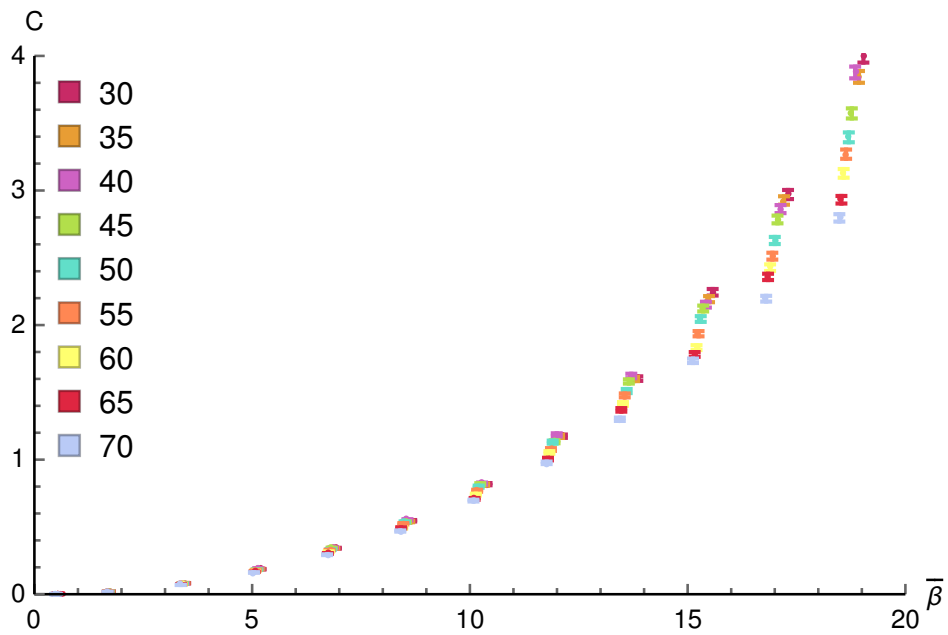


Figure 21: The specific heat  $C$  plotted against  $\bar{\beta}$  for  $\epsilon = 0.21$  on either side of the phase transition.

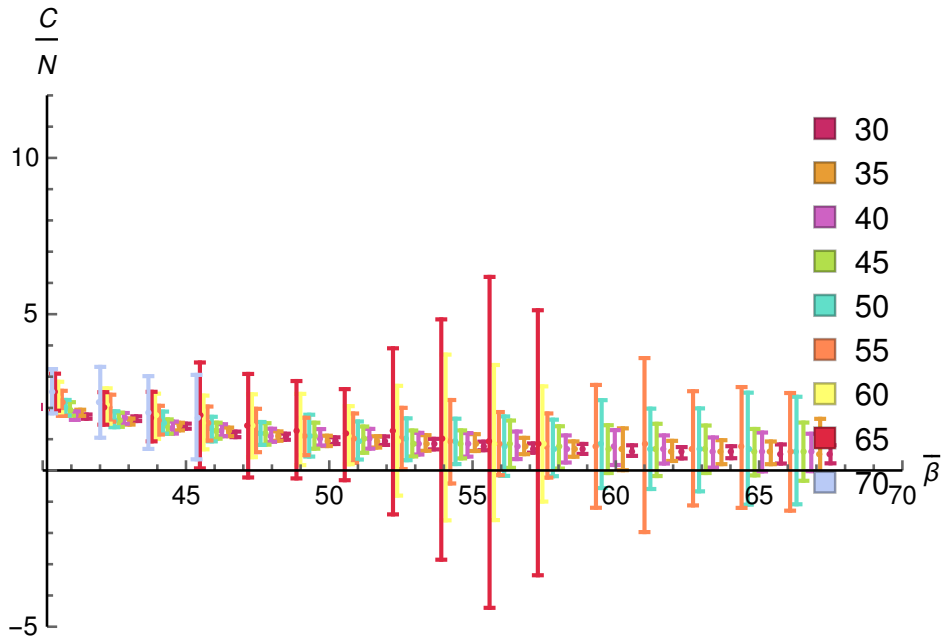


Figure 22: Recaling  $C$  by  $N$  leads to a very good collapse of the values for all  $N$ .

### 4.3 First Order Phase Transition

In Figure 23 we focus on  $\beta\langle S \rangle$  around the phase transition. We find that as  $N$  increases the transition becomes sharper with  $N$  suggesting a discontinuous or first order transition.

Examining the raw data, we are able to extract the double Gaussians that characterise first order phase transitions, as shown in Figure 24 at the estimated  $\beta_c$  for  $\epsilon = 0.21$ . However, as pointed out in [18], for finite  $N$  these features alone are not sufficient to establish conclusively that the transition is first order. This is *only* established once we look at the double Gaussians as a function of  $N$ . Figure 24 shows the separation between the peaks increasing with  $N$ , which we find is the strongest evidence for a first order phase transition.

We also analyse the scaling of the peaks of the specific heat  $C$ . Since  $\nu_+ = 1 > \nu_- = 0$ , we expect the scaling at the first order transition to go as  $2\nu_+ = 2$ . As shown in Figure 25 this is indeed the case.

Another marker to explore the order of a phase transition is the so called Binder cumulant<sup>2</sup>

$$B = \frac{1}{3} \left( 1 - \frac{\langle S^4 \rangle}{\langle S^2 \rangle^2} \right). \quad (30)$$

At fixed  $N, \epsilon$  this quantity has a minimum at the pseudocritical point, and as shown in [18] it takes on a non-zero negative value at first order transitions, and is zero for second

<sup>2</sup>This is shifted by 2/3 from the standard definition.

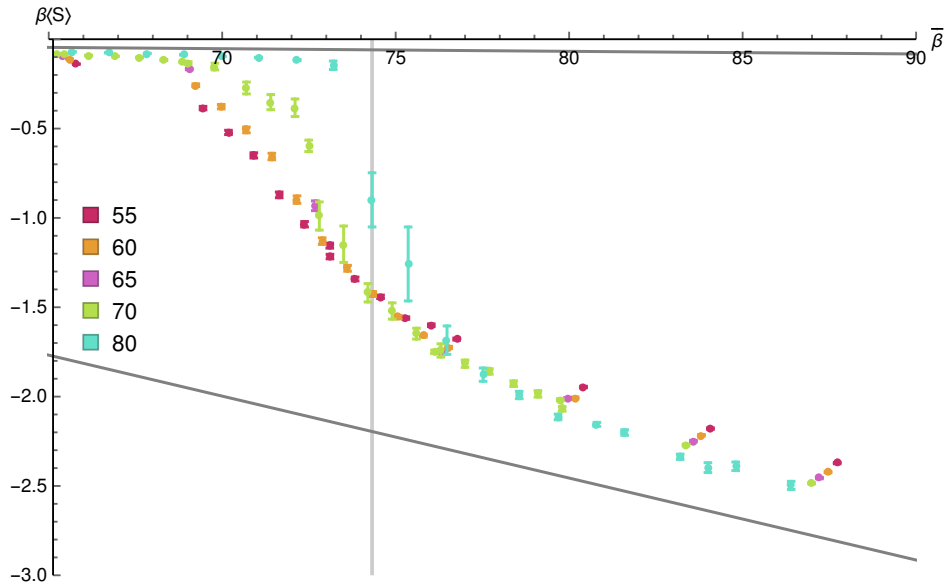


Figure 23: In the region of the phase transition, it is clear that as  $N$  increases,  $\langle S \rangle$  becomes more and more discontinuous. Here we have plotted the fit functions for  $\langle S \rangle$  before and after the phase transition to demonstrate the discontinuity.

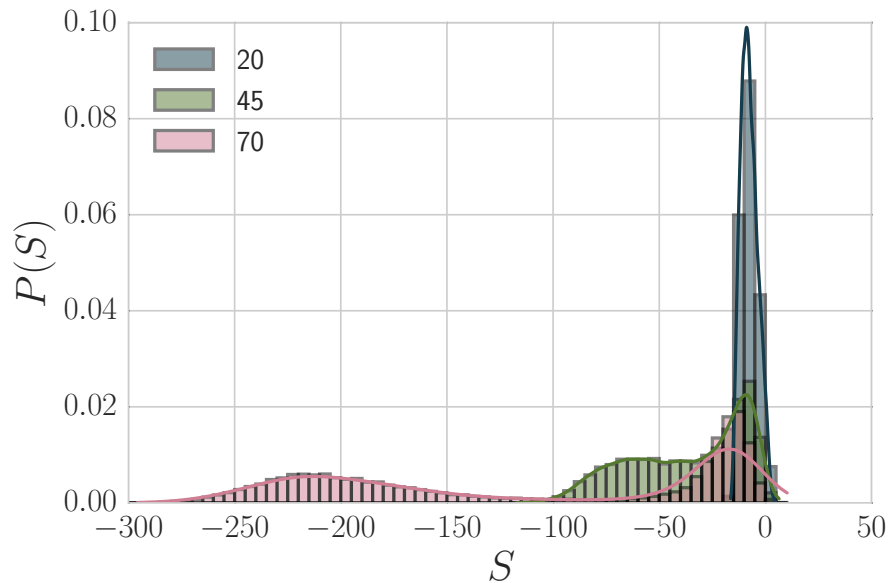


Figure 24: Plotting all measured values of  $S$  into a histogram shows that at  $\beta_c$  the histogram splits into two peaks which wander further away from each other as  $N$  increases.

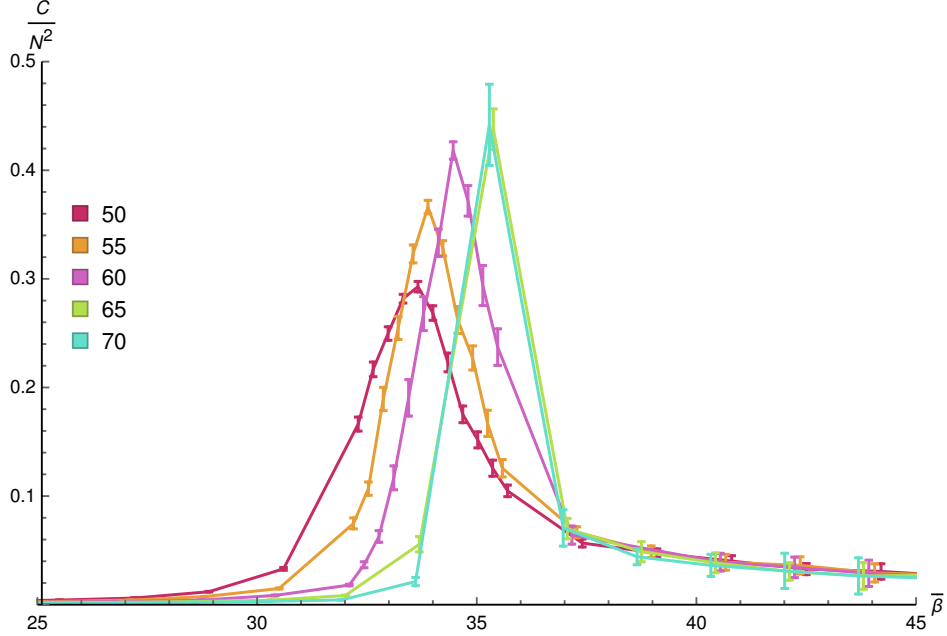


Figure 25: We show the rescaling of the peak values of  $C$  by  $N^2$  to converge for larger  $N$ . Here  $\epsilon = 0.21$ .

order transitions. While in finite size systems some deviation from 0 is expected, this can be determined by observing the trend as  $N$  is increased.

The double Gaussian Eqn (11) predicts for  $N \rightarrow \infty$  and  $p_+ = t, p_- = 1 - t$ , assuming that  $\mu_+ > \mu_-$  that  $B = \frac{1}{3} - \frac{t+(1-t)x^4}{3(t+(1-t)x^2)^2}$ , where  $x \equiv \frac{\mu_-}{\mu_+}$ . When the Gaussians are equally weighted ( $t = \frac{1}{2}$ ),  $B$  lies between 0 and  $-\frac{1}{3}$ .

To be able to determine the minimum value of the Binder coefficient with reasonable precision, we used a reweighting procedure, as explained in [20] to approximate the value of  $B$  in the region where we expected the pseudocritical point. We plot this observable against the inverse system size in figure 26, and can clearly see that it tends to a non-zero value. Taking  $\mu_+ = \langle S_+ \rangle \sim N^2, \mu_- = \langle S_- \rangle \sim N$  gives  $B \sim \frac{1}{3} - \frac{1}{3t}$  for large  $N$ . For larger  $N$ , we see that  $t \sim 0.04$ , which suggests that we have not sampled the immediate vicinity of the critical point with sufficient precision. Alternatively it may be due to the asymmetry of scaling on either side of the phase transition. In either case, Fig 26 provides additional supporting evidence for a first order phase transition.

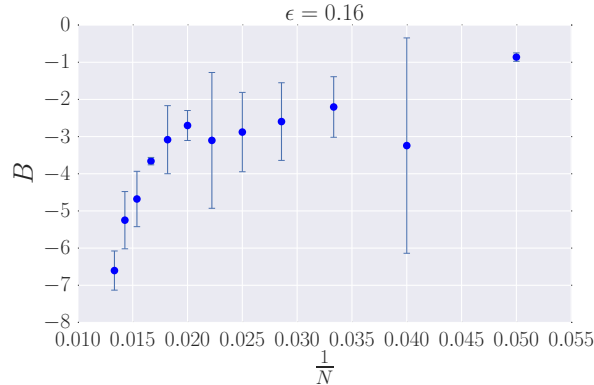


Figure 26: The Binder coefficient moves further away from 0 as  $N$  becomes larger, thus indicating a first order phase transition.

## 5 Conclusions and Open Questions

The most unexpected and physically interesting outcome of our analysis is the possible generation, of a negative non-zero cosmological constant  $\Lambda$  associated with the constant curvature spacetime  $adS_2$ . The scale of  $\Lambda$ , moreover, is simply set by  $\epsilon$  and  $\bar{\beta}$ , via the relation

$$\Lambda = \kappa_2 b_1^-(\epsilon) \bar{\beta}, \quad (31)$$

where  $\kappa_2 \sim l_p^{-2}$ . While there is no *natural* Planck scale in 2d, given a scale,  $\Lambda$  can be made as small as desired by choosing  $\bar{\beta}$  to be small enough.

Apart from the extensivity of the action, there are other indications that a typical causal set in this phase is approximated by a causal patch of  $adS_2$ . The Myrheim-Myer (MM) flat spacetime dimension is given by the inverse of the ordering fraction  $f_r = r/\binom{N}{2}$  where  $r$  denotes the number of relations [21, 22]. In our simulations we have generated this ordering fraction alongside the action. We find that in the continuum phase, our data shows that  $f_2 \sim 0.5$  resulting in an MM flat spacetime dimension of  $\sim 2$ , which lends support to this being a continuum phase.

Additionally, in our simulations we have generated and saved actual configurations, which allows us to extract other observables of interest, like the abundance of intervals  $\langle N_n \rangle$ . We find that up until the phase transition they satisfy the expected continuum behaviour ([23]) as seen in Fig 27(a)-(c). For very small  $\beta$  in Fig 27(a) the abundance curve simply tracks that of flat spacetime. However, as  $\beta$  increases,  $\beta < \beta_c$ , the abundance curve dips below that of flat spacetime as shown in Figure 27(b). While we do not at present have an exact comparisons with sprinklings into  $adS$  spacetime, we note that Figure 12 of [23] shows that for positive  $\Lambda$ , i.e., de Sitter spacetime, the curve rises above the flat spacetime curve, while

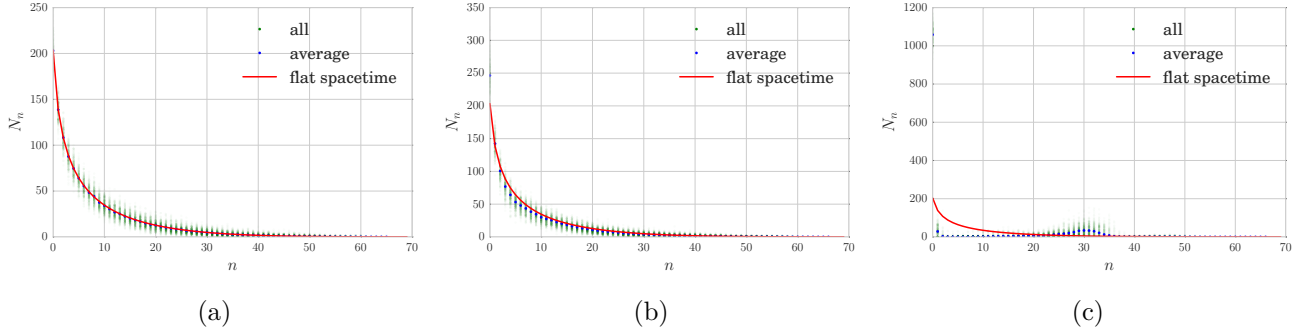


Figure 27: For the smallest values of  $\bar{\beta}$  the abundance of intervals is indistinguishable from flat spacetime (a), but begins to deviate as  $\bar{\beta}$  is increased (b). After the phase transition(c), the deviation is very pronounced and corresponds to the crystalline phase

the curves of matter and radiation dominated FRW dip below this curve. Thought of as a positive pressure, the negative  $\Lambda$  therefore seems compatible with the latter.

In the above analysis we have probed thermodynamic quantities, which can frequently be reliably obtained from small systems. This is due to the existence of a limiting free energy whose finite size corrections fall off with inverse powers of  $N$ . Our analysis suggests a clear approach to the asymptotic regime by  $N \gtrsim 65$  for 2d CST. Given that we refer to phase  $\Pi_-$  as a “continuum” phase, this might seem surprisingly small to recover continuum behaviour, but this can be traced to the non-locality in the causal set. For example, in a simplicial decomposition or triangulation of 2d spacetime, the valency of the dual graph is 3 and so the amount of information contained in an  $N$  element simplex grows like  $3N \sim O(N)$ . It is only by increasing this (local) *information* that one can hope to find continuum-like behaviour.

On the other hand non-locality implies that that the information in a causal set can be very much larger than the  $O(N)$  suggested by its cardinality. The information in a causal set approximated by flat spacetime is contained in the abundance profile  $\langle N_n \rangle$  v/s  $n$ , where  $\langle N_n \rangle \sim N \ln N$  in the asymptotic limit for 2d spacetimes, with order  $N$  corrections [23]. The simultaneous imposition of this form on each  $n$  grows at a *minimum* as  $N \ln N$ . An exact estimation of this is out of the scope of the present paper.

Finally we note that our discussion of the large  $\beta$  limit generalises to the BD action in any dimension, which has a function similar to  $f(n, \epsilon)$  with a maximum at  $n = 0$ . Hence configurations with the maximum number of links will have the smallest action and hence the lowest energy. If we consider the full sample space of  $N$  element causal sets, there is an entropic dominance of so-called Kleitman-Rothschild(KR) posets which have three layers and hence are non-manifold like. Their density of states goes as  $\sim 2^{\frac{N^2}{4}}$  for large  $N$  [15]. On the other hand, the number of links in each KR poset  $N_0 \sim N^2/8$  with the next significant abundance being for  $n = N/4$ , whose contribution to the action is highly suppressed by

$f(n, \epsilon)$  for large enough  $\epsilon$ . Thus the contribution of the KR posets  $\sim 2^{\frac{N^2}{4}} e^{+\beta\epsilon^2 N^2}$  which for large enough  $\beta$  is subdominant to the contribution from the bilayer posets  $\rho_b(\beta, N, \epsilon) e^{+2\beta\epsilon^2 N^2}$ , Equation (7). Hence we predict that the large  $\beta$  phase will be dominated by the bilayer posets for the class of statistical partition functions defined by the BD action in any dimension.

## 6 Acknowledgements

We thank David Rideout for help with Cactus. The simulations were performed using the Cactus Causal Set Toolkit [24, 25]. This work has been supported by COST Action MP1405 “Quantum structure of spacetime (QSPACE). LG has received funding from the People Programme (Marie Curie Actions) H2020 REA grant agreement n.706349 "Renormalisation Group methods for discrete Quantum Gravity". This research was supported in part by Perimeter Institute for Theoretical Physics. Research at Perimeter Institute is supported by the Government of Canada through the Department of Innovation, Science and Economic Development and by the Province of Ontario through the Ministry of Research and Innovation. SS was also supported in part under an agreement with Theiss Research and funded by a grant from the FQXI Fund on the basis of proposal FQXi-RFP3-1346 to the Foundational Questions Institute. SS is currently supported by FQXi-MGA-1510 and an Emmy Noether Fellowship, at the Perimeter Institute.

## References

- [1] Luca Bombelli, Joochan Lee, David Meyer, and Rafael Sorkin. Space-Time as a Causal Set. *Phys.Rev.Lett.*, 59:521–524, 1987.
- [2] Sumati Surya. Evidence for the continuum in 2d causal set quantum gravity. *Classical and Quantum Gravity*, 29(13):132001, July 2012.
- [3] Lisa Glaser and Sumati Surya. The Hartle–Hawking wave function in 2D causal set quantum gravity. *Class. Quant. Grav.*, 33(6):065003, 2016.
- [4] Joe Henson, David Rideout, Rafael D. Sorkin, and Sumati Surya. Onset of the asymptotic regime for (uniformly random) finite orders. *Experimental Mathematics*, 26(3):253–266, 2017.
- [5] Luca Bombelli, Joe Henson, and Rafael D. Sorkin. Discreteness without symmetry breaking: A Theorem. *Mod.Phys.Lett.*, A24:2579–2587, 2009.
- [6] Alessio Belenchia, Dionigi M. T. Benincasa, Eduardo Martin-Martinez, and Mehdi Saravani. Low energy signatures of nonlocal field theories. *Physical Review D*, 94(6):061902, September 2016.

- [7] Mehdi Saravani and Niayesh Afshordi. Off-shell dark matter: A cosmological relic of quantum gravity. *Physical Review D*, 95(4):043514, February 2017.
- [8] Rafael D Sorkin. Is the spacetime metric Euclidean rather than Lorentzian? *arXiv:0911.1479*, November 2009.
- [9] M. El-Zahar and N. W. Sauer. Asymptotic enumeration of two-dimensional posets. *Order*, 5(3):239–244, September 1988.
- [10] Peter Winkler. Random orders of dimension 2. *Order*, 7(4):329–339, December 1990.
- [11] Rafael D. Sorkin. Space-time and causal sets. 1990.
- [12] Sumati Surya. Directions in Causal Set Quantum Gravity. In A. Dasgupta, editor, *Recent Research in Quantum Gravity*. Nova Science Publishers, NY, 2013.
- [13] Rafael D. Sorkin. Causal sets: Discrete gravity. In *Lectures on quantum gravity. Proceedings, School of Quantum Gravity, Valdivia, Chile, January 4-14, 2002*, pages 305–327, 2003.
- [14] Graham Brightwell, Joe Henson, and Sumati Surya. A 2d model of causal set quantum gravity: the emergence of the continuum. *Classical and Quantum Gravity*, 25(10):105025, May 2008.
- [15] D. J. Kleitman and B. L. Rothschild. Asymptotic enumeration of partial orders on a finite set. *Transactions of the American Mathematical Society*, 205:205–220, 1975.
- [16] Dionigi M.T. Benincasa, Fay Dowker, and Bernhard Schmitzer. The Random Discrete Action for 2-Dimensional Spacetime. *Class.Quant.Grav.*, 28:105018, 2011.
- [17] Michel Buck, Fay Dowker, Ian Jubb, and Sumati Surya. Boundary Terms for Causal Sets. *Classical and Quantum Gravity*, 32(20):205004, October 2015. arXiv: 1502.05388.
- [18] Murty S. S. Challa, D. P. Landau, and K. Binder. Finite-size effects at temperature-driven first-order transitions. *Physical Review B*, 34(3):1841–1852, August 1986.
- [19] Charles Nash and Denjoe O’Connor. Topological Phase Transitions and Holonomies in the Dimer Model. *J. Phys.*, A42:012002, 2009.
- [20] M. E. J. Newman and G. T. Barkema. *Monte Carlo Methods in Statistical Physics*. Clarendon Press, February 1999.
- [21] J. Myrheim. STATISTICAL GEOMETRY. 1978.
- [22] David A. (David Alan) Meyer. The dimension of causal sets. 1988. Thesis (Ph. D.)–Massachusetts Institute of Technology, Dept. of Mathematics, 1989.

- [23] Lisa Glaser and Sumati Surya. Towards a Definition of Locality in a Manifoldlike Causal Set. *Phys.Rev.*, D88:124026, 2013.
- [24] T. Goodale, G. Allen, G. Lanfermann, J. Massó, T. Radke, E. Seidel, and J. Shalf. The Cactus framework and toolkit: Design and applications. In *Vector and Parallel Processing — VECPAR 2002, 5th International Conference*, pages 197–227, Berlin, 2003. Springer.
- [25] G. Allen, T. Goodale, F. Löffler, D. Rideout, E. Schnetter, and E. L. Seidel. Component specification in the Cactus Framework: The Cactus Configuration Language. pages 359–368, October 2010.